Platinum nanoparticles supported on functionalized hydroxyapatite: Anti-oxidant properties and bone cells response

Platinum nanoparticles supported on functionalized hydroxyapatite: anti-oxidant properties and bone cells response

Elisa Boanini[a,*], Paola Torricelli[b], Maria Cristina Cassani[c,*], Katia Rubini[a], Milena Fini[b], Stefania Pagani[b], Adriana Bigi[a]

Affiliations:

[a] Department of Chemistry ‘‘G. Ciamician”, University of Bologna, via Selmi 2, 40126 Bologna, Italy

[b] IRCCS Istituto Ortopedico Rizzoli, Laboratorio Studi Preclinici e Chirurgici, 40136 Bologna, Italia

[c] Department of Industrial Chemistry “Toso Montanari”, University of Bologna, Via del Risorgimento, 4, 40136 Bologna, Italy

Corresponding authors:

[*] Prof. Elisa Boanini; e-mail: elisa.boanini@unibo.it ; Tel: +39 051 2099548

[*] Prof. Maria Cristina Cassani; e-mail: maria.cassani@unibo.it ; Tel: +39 051 2093700

Abstract

Platinum ions and nanoparticles applications in the biomedical field include a number of pathologies. In particular, platinum ions are useful in the preparation of antitumoral drugs, whereas Pt nanoparticles (PtNPs) are known to reduce cellular oxidative stress. Herein, we developed composite materials using poly(ethylenimine) functionalized hydroxyapatite (HAPEI) as support for platinum. The presence of polyelectrolyte promotes interaction with platinum ion, which is loaded in greater amount than on pure hydroxyapatite. The dimensions of PtNPs are very small (about 1 nm), but increase up to about 20-30 nm on heat treatment. Loading Pt(II) ion on the apatitic supports provide a material with cytotoxic properties towards osteosarcoma derived cell lines (SaOS2 and MG63). On the contrary, PtNPs loaded apatitic supports display good anti-oxidant properties, in agreement with their quenching activity towards H_2O_2. Moreover, they promote differentiation of both primary osteoblast and osteoblast cell line, as shown by the increase of the levels of Alkaline Phosphatase and Collagen type 1, and reduce the level of reactive oxygen species with a consequent decrease of cellular oxidative stress.

Keywords: platinum; hydroxyapatite; oxidative stress; osteosarcoma cell lines; primary osteoblasts

1. Introduction

Platinum compounds and nanoparticles are applied in several different fields. The high efficiency as antitumoral agents of its coordination compounds, as the cis-platinum complex, is well known [1]. Moreover, platinum nanoparticles (PtNPs) are used in fuel cells [2], catalysis and photocatalysis [3-5], as well as in water treatment processes for the removal of problematic pharmaceutical products [6]. In the biomedical field, PtNPs have been reported to be useful in a variety of pathologies, including pulmonary inflammation, cancer and vascular diseases [7-11]. Moreover, they can quench hydrogen peroxide and superoxide, exhibiting a behavior similar to that of the catalase and superoxide dismutase enzymes, and reduce cellular oxidative stress [12,13].

The use of hydroxyapatite (HA) as support for PtNPs should provide functionalized materials useful for the regeneration and replacement of bone tissue. In fact, thanks to its excellent biocompatibility and bioactivity, HA is the most employed calcium phosphate for the preparation of biomaterials for the treatment of defects of the musculo-skeletal system [14]. The use of HA as support for PtNPs has been explored for catalytic applications [3-5, 15], whereas the biological performance of these materials has not been investigated up to now.

This work focuses on the functionalization of hydroxyapatite nanocrystals with platinum and on the investigation of their influence on tumoral and normal bone cells biocompatibility and differentiation. In order to provide a more attractive surface, we used HA nanocrystals functionalized with poly(ethylenimine) (PEI) as supports. PEI is a cationic polymer which displays a high affinity with negatively charged species [16]. Moreover, it contains a great number of ionizable amino groups that allow to bind to substrates and chelate metallic ions [17]. In particular, we employed low molecular weight PEI, which does not give citotoxicity problems, and compared the results with those obtained for pure HA [18-20].

2. Materials and methods

2.1 Synthesis and characterization

HA nanocrystals were synthesized in N_2 atmosphere using 50 ml of a solution containing 1.08M $Ca(NO_3)_2 \cdot 4\ H_2O$, prepared with CO_2-free water. The solution was heated at 90 °C and pH adjusted to 10 with NH_3 (28-30 wt%). Afterwards 50 ml of 0.65M $(NH_4)_2HPO_4$ solution was added drop-wise (approx. 20 min) under stirring. The precipitate was maintained in contact with the reaction solution for 5 hours at 90 °C under stirring, then centrifuged at 10,000 rpm for 10 minutes and repeatedly washed with distilled water. The product was dried at 37 °C overnight, and then mildly ground in an agate mortar and sieved (d = 40 μm).

HAPEI nanocrystals were prepared following the above procedure, but starting from a solution containing 1.08M $Ca(NO_3)_2 \cdot 4\ H_2O$ and 8M poly(ethylenimine) (Aldrich, MW ~ 2000 g mol^{-1}).

HA and HAPEI specific surface area was measured using a Carlo Erba Sorpty 1750 BET analyzer using constant volume N_2 adsorption with desorption at 80°C.

For the preparation of the samples loaded with Pt(II) (HA-PtNR and HAPEI-PtNR), 0.500 g of freshly sieved apatitic powder was suspended in 12.5 ml of MilliQ water under stirring. After addition of 12.5 ml of 0.01M K_2PtCl_4 (> 98%, Strem Chemicals Inc.) solution, stirring was maintained for 1 hour at RT, afterwards powder was isolated by filtration on a funnel buckner and dried at 37°C. The successive reduction of Pt(II) containing samples was carried out on 0.500 g of powder (HA-PtNR and HAPEI-PtNR), that were suspended into 5 ml of MilliQ water. Subsequently 20 ml of a 0.1 M aqueous solution of $NaBH_4$ (99%, Sigma Aldrich) was added to the suspension under stirring for 30 min at RT. Then the samples (HA-PtR and HAPEI-PtR) were filtered, washed with water, and dried at 37°C.

HA-PtTT and HAPEI-PtTT were obtained after heat-treatment of HA-PtR and HAPEI-PtR at 700 °C for 4 hours. Although heat treatment provoked complete removal of the polyelectrolyte, the label HAPEI-PtTT was maintained to distinguish these samples from those obtained through heat treatment of HA-PtR (HA-PtTT).

Powder X-ray diffraction (XRD) patterns were recorded using a PANalytical X'Pert PRO powder diffractometer equipped with a fast X'Celerator detector. CuKα radiation was used (λ = 0.154 nm, 40 mA, 40 kV). For phase identification the 2θ range was investigated from 10 to 60 2θ degrees with a step size of 0.1° and time/step of 100 s.

The amount of platinum present on the different samples was determined by flame atomic absorption spectroscopy (AAS, THERMO iCE 3000 Series) in air-acetylene flame with a wavelength of 266.0 nm. For this analysis ca. 5 mg of sample were dissolved in 25 ml of a 0.5 M HNO_3 (NORMATOM®) aqueous solution adding, when necessary, small amounts of aqua regia until complete dissolution. The calibration line was made with 5 calibration standards (2, 4, 6, 8, 10 ppm) prepared by dilution with 0.5 M HNO_3 of a platinum standard for AAS (TraceCERT®, Merck, 1000 ± 4 ppm Pt in 5 % HCl). Results from this analysis represent the mean value of three different determinations.

Thermogravimetric analysis was performed using a Perkin‑Elmer TGA-7, heating samples (5‑10 mg) in a platinum crucible in air flow (20 cm^3/min) at a rate of 10 °C/min up to 600 °C.

For Transmission Electron Microscopy (TEM) investigations, a small amount of powder was dispersed in ethanol and submitted to ultrasonication. A drop of the suspension was transferred onto holey carbon foils supported on conventional copper microgrids. A Philips CM 100 transmission electron microscope operating at 80 kV was used.

The hydrogen peroxide scavenging activity of HAPEI-PtR, HAPEI-PtTT and HAPEI for comparison was determined with the Pierce™ Quantitative Peroxide Assay Kit (Thermo Scientific). Peroxide standards were obtained after serially diluting a 30% (8.8M) hydrogen peroxide stock solution to achieve 8 standards in the concentration range of 7.8-1000μM. Tests were performed on disk-shaped samples (Ø = 6.0 mm), prepared by pressing 40 mg of powder into cylindrical moulds by using a standard evacuable pellet die (Specac) at 10 tons. Each disk was immersed in 125 μM H_2O_2 at 37°C. The pH value was kept constant at 7.4 with 0.15M phosphate buffered saline (PBS). A 20 μL aliquot was taken from the reaction solution after 30 min, 1, 2, 3, 4, 5, 6 and 7 hours and its residual H_2O_2 was determined with the addition of 200 μL Assay Kit working reagent in microplate wells. Absorbance was measured at 550 nm using a plate reader.

2.2 In vitro tests

Samples of HAPEI-PtNR, HAPEI-PtR and HAPEI-PtTT were prepared for in vitro tests. Disk shaped samples (diameter = 6 mm, height = 1.5 mm) were prepared by pressing 40 mg of powder into cylindrical molds by using a standard evacuable pellet die (Hellma). Before in vitro tests, the samples were sterilized by gamma irradiation (25 kGy). The cells were cultured in direct contact with the disk shaped samples.

2.2.1 Cytotoxicity test

A preliminary test of cytotoxicity was performed using MG63 cell line (Istituto Zooprofilattico Sperimentale IZSBS, Brescia, Italy). Cells ($5x10^4$cells/well) were tested after 48 hours of culture with HAPEI-PtNR, HAPEI-PtR and HAPEI-PtTT (three samples each), in DMEM medium (Dulbecco's Modified Eagle's Medium, Sigma, UK, supplemented with 10% FCS, and antibiotics - 100 U/ml penicillin, 100 μg/ml streptomycin), together with CTR– (cells and DMEM only as negative control), and CTR+ (cells and 0.05% phenol solution in DMEM as positive control). Cell viability

was assessed by WST1 (WST1, Roche Diagnostics GmbH, Manheim, Germany) colorimetric reagent test. The assay is based on the reduction of tetrazolium salt into a soluble formazan salt by a reductase of the mitochondrial respiratory chain, active only in viable cells. 100 μl of WST1 solution and 900 μl of medium (final dilution: 1:10) were added to the cell monolayer, and the multi-well plates were incubated at 37°C for a further 4 h. Supernatants were quantified spectrophotometrically at 450 nm with a reference wavelength of 625 nm. Results of WST1 are reported as optical density (OD) and directly correlate with the cell number. Proliferation percent relative to CTR− (considered as 100%) was also calculated. A further analysis for cell viability was performed by Live/Dead® assay (Molecular Probes, Eugene, OR, USA), according to the manufacturer's instructions. Samples were visualized using an inverted microscope equipped with an epifluorescence setup (Eclipse TiU, NIKON Europe BV, NITAL SpA, Milan, Italy): excitation/emission setting of 488/530 nm to detect green fluorescence (live cells) and 530/580 nm to detect red fluorescence (dead cells). At the same fixed time point, the supernatants of each well was collected, and centrifuged to remove particulates, to measure Lactate Dehydrogenase (LDH detection kit, Roche diagnostics, IN, USA), enzyme released in medium when cell membrane is damaged. The test was performed following manufacturer's instruction and LDH concentration was spectrophotometrically read and reported as percentage of CTR.

To further confirm the cytotoxic properties of HAPEI-PtNR, a cytotoxicity test was repeated using osteoblast-like cell line derived from osteosarcoma SaOS2 and MG63 (IZSBS, Brescia, Italy). Cells were cultured in DMEM medium. Both cell lines were plated at a concentration of $5x10^4$cells/well in 24-well plates containing six sterile samples each of HAPEI-PtNR, CTR–, CTR+, and HA as reference. Plates were cultured in standard conditions, at 37 ± 0.5°C with 95% humidity and 5% ± 0.2 CO_2 up to 48 hours.

The quantitative and qualitative evaluation of cytotoxicity was performed by measuring cell viability and membrane damage. Cell viability at 48 hours was assessed by Alamar blue dye (Cell Viability Reagent, LIFE Technologies Corp., Oregon, USA): the reagent was added (1:10 v/v) to each well and incubated for 4 hours at 37°C. A redox indicator, incorporated in the reagent, changes its color in response to the chemical reduction of the medium resulting from living cells. The result is expressed as relative fluorescence units (RFU). Live/Dead® assay and LDH measure were also performed, as described above.

2.2.2 Bioactivity test

Primary osteoblast NHOst (Lonza Walkersville Inc., Belgium) and osteoblast cell line MG63 were previously expanded in DMEM, counted and plated at a concentration of $2x10^4$cells/well in 24-well plates containing six sterile samples of HAPEI-PtR, HAPEI-PtTT, and HA as reference each type of cells. Plates were cultured in standard condition with DMEM supplemented with β-glicerophosphate (10^{-4}M) and ascorbic acid (50 μg/ml), changing medium every other days for 10 days.

At 3, 7 and 10 days viability was assessed by means of Alamar blue reagent and Live/Dead® assay (methods previously described). At the end of experimental times supernatants of all wells were collected, centrifuged to remove particulates if any, and aliquots were dispensed in Eppendorf tubes for storage at -70°C to be assayed with the following immunoenzymatic kits: Alkaline Phosphatase and Collagen type 1 (ALP, COL1a1, Cloud-Clone Corp., Wuhan, China), Reactive Oxigen Species (ROS, MyBioSource, CA, USA) and Reactive Oxigen Modulator 1 (ROMO1, Cloud-Clone).

3. Results and discussion

3.1 Chemical and structural characterization

The synthesis of hydroxyapatite in the presence of 4M PEI produces a single crystalline phase (HAPEI) which exhibits a powder XRD pattern close to that of pure HA, as shown in Figure 1a. Polyelectrolyte content in HAPEI can be determined by comparing its thermogravimetric (TG) plot with that of HA [21]: the different weight losses of the two compounds up to about 600°C (Figure 1b) can be ascribed to the presence of PEI, which amounts to about 5.2 wt%.

In this work we used HA and HAPEI crystals as supports for the loading of Pt(II) ions, which give rise to the formation of supported PtNPs after following reduction reaction (Figure 2).

The presence of PtNPs on the two different supports can be appreciated in the TEM images recorded after platinum reduction. The images reported in Figure 3 show that the number of PtNPs on HA-PtR is much less than those on HAPEI-PtR. These data are supported by the results of chemical analyses, which indicate that the amount of Pt adsorbed onto HA and HAPEI are 0.7 wt% and 2.2 wt%, respectively, with no significant differences before and after reduction. Since HA and HAPEI display similar specific surface areas, 23 and 26 m^2/g respectively, the greater amount of Pt(II) or PtNPs loaded on HAPEI in comparison to HA, must be attributed to the presence of the polyelectrolyte, which promotes interactions with the metallic ion [22].

In both supports, PtNPs display very small dimensions, of the order of magnitude of 1 nm. Heat treatment of HA-PtR and HAPEI-PtR samples at 700 °C induces complete removal of PEI and aggregation of Pt nanoparticles, which display significantly bigger dimensions, up to about 20-30 nm as shown in Figure 3 for HAPEI-PtTT. These dimensions are sufficient to allow to appreciate the presence of Pt in the relative X-ray diffraction patterns: as shown in Figure 4, the XRD pattern of HAPEI-PtTT displays the

typical reflections of HA (PDF n. 9-432) together with a peak at about 40°/2θ and a shoulder at about 46°/2θ, characteristic of Pt (PDF n. 01-087-0646). On the contrary, these features cannot be appreciated in the XRD patterns of the samples before heat treatment. In agreement with the very small dimensions of PtNPs, the XRD pattern of HAPEI-PtR shows just a diffuse halo centered around 40°/2θ (Figure 4). As expected, the pattern of HAPEI-PtNR is similar to that observed before platinum loading. Magnification of the XRD patterns in the relevant range of 2θ allows to enhance these differences, as shown in Figure S1. Similar results were obtained for the samples prepared using HA as support (Figure 4, Figure S1).

PtNPs are known to display anti-oxidant properties [12]. In order to verify if the anti-oxidant power is maintained when the nanoparticles are supported on apatitic crystals, we tested the quenching activity of HAPEI-PtR and of HAPEI-PtTT against H_2O_2 and compared the results with those obtained for HAPEI (Figure S2). The data reported in Figure 5 show that the presence of HAPEI in solution causes elimination of only about 10% of hydrogen peroxide after 7 hours. On the contrary, both HAPEI-PtR and HAPEI-PtTT can eliminate about 20% of H_2O_2 in just 30 minutes. Moreover, approximately 100% of H_2O_2 can be decomposed in 7 hours in the presence of HAPEI-PtR or HAPEI-PtTT, indicating that both materials possess a high activity for scavenging hydrogen peroxide.

3.2 In vitro tests

As for the quenching activity against H_2O_2, in vitro tests were performed on the series of samples obtained using HAPEI as support, because of their greater platinum content than the HA series.

3.2.1 Cytotoxicity

In the preliminary test of cytotoxicity, after 48 hours of culture on HAPEI-PtNR, osteoblast cell viability dramatically decreased and LDH release was significantly high ($p<0.0005$), as shown in Figure S3. On the contrary, the viability on HAPEI-PtR and HAPEI-PtTT was even greater than on CTR-, and the relative values of LDH release were very low, demonstrating complete absence of citotoxicity. The different cytotoxic behavior of HAPEI-PtNR when compared to HAPEI-PtR and HAPEI-PtTT were confirmed by the images of Live/Dead® fluorescent staining (Figure S4).

Further investigation on HAPEI-PtNR with both SaOS2 and MG63 cell lines confirmed the preliminary data: the comparison with CTR- and HA demonstrated a significantly reduced viability of SaOS2 and MG63 ($p<0.0005$). HA group viability did not differ from CTR- in MG63, and was significantly higher in SaOS2 ($p<0.05$), (Figure 6). The cytotoxic effect of HAPEI-PtNR was further confirmed also by the measure of LDH in supernatant (Figure 6): LDH release was significantly higher in HAPEI-PtNR group then in CTR- and HA, for both SaOS2 and MG63cell lines ($p<0.0005$ and $p<0.005$ respectively). No significant differences were found between CTR- and HA reference groups. The results of cell viability were in line with the images detected after Live/Dead® fluorescent staining (Figure 7). The images showed a good viability of both type of cells on HA (green color), while on HAPEI-PtNR a majority of dead cells (red color) can be observed.

SaOS2 and MG63 are two osteosarcoma derived cell lines, that express different phenotypes, SaOS2 exhibiting a more mature osteoblastic phenotype in comparison with that of MG63. Both of them present advantages for in vitro culture (human, easy availability, reliable reproducibility, etc) and they are widely used as useful in vitro models to test cytotoxicity and biocompatibility of implant materials. The present results demonstrate that HAPEI-PtNR, unlike HAPEI-PtR and HAPEI-PtTT, may be

considered an antitumoral active agent, inducing a significant cytotoxic effect on osteosarcoma derived cell lines.

3.2.2 HAPEI-PtR and HAPEI-PtTT bioactivity

Preliminary cytotoxicity tests showed that HAPEI-PtR and HAPEI-PtTT did not affect cell viability and that they were suitable to study cell activity and differentiation with primary bone cells. The biological effects of HAPEI-PtR and HAPEI-PtTT on NHOst and MG63 osteoblasts were tested after 10 days of culture. NHOst are primary osteoblast, used at the second passage and able to maintain their differentiation and to mineralize. NHOSt were tested in parallel with MG63 cell line for comparison. Viability on HA reference samples is regular in both type of cells. MG63 grown on HAPEI-PtR and HAPEI-PtTT does not show differences when compared to those grown on HA, except for a slight slowdown of HAPEI-PtTT when compared to HA at 10 days ($p<0.05$), compatible with differentiation and metabolic activity. On the contrary the proliferation of NHOst on HAPEI-PtR and HAPEI-PtTT is lower in comparison with HA group (Figure 8), even if the differences are significant only for HAPEI-PtR group ($p<0.005$ at 3, 7 and 10 days).

Images of Live/Dead® fluorescent staining in Figure 9 show cell colonization on experimental samples demonstrating no alteration of the normal cell morphology. The density of cells correlates with viability data.

At the fixed experimental time-points, ALP and COL1a1, as common markers of osteoblast differentiation, were measured to investigate metabolic activity (Figure 10). The results of ALP in NHOst show that at 3 days ALP activity on both HAPEI-PtR and HAPEI-PtTT is lower than on HA ($p<0.05$), with HAPEI-PtTT higher than HAPEI-PtR ($p<0.05$). At variance, at 7 days the values on HAPEI-PtR and HAPEI-PtTT are significantly higher in comparison to HA. No differences among groups were found at

10 days. The results of MG63 on HAPEI-PtR and HAPEI-PtTT are higher than on HA at all experimental time ($p<0.05\%$).

COL1a1 produced by NHOst on HAPEI-PtR group is always lower than on HA ($p<0.05$), whereas no significant differences can be found between HAPEI-PtR and HA production by MG63. The production of COL1a1 by NHOst on HAPEI-PtTT is lower than on HA at 3 days ($p<0.05$), but its levels increase with time so that no difference was recorded at 7 days, whereas it was higher at 10 days ($p<0.05$). MG63 production of COL1a1 on HAPEI-PtTT is significantly higher than on HA and HAPEI-PtR ($p<0.05$) at all experimental times.

The effect of the different materials on cellular response to oxidative stress was investigated through ROS and ROMO1 assays. The production of ROS depends on various mechanisms of exogenous and endogenous sources. Their damaging actions, when an overproduction occurs, may affect protein and lipid as well as nucleic acids, contributing to cell senescence [23]. ROMO1 is a modulator responsible for increasing the production of ROS and it plays a role in inducing DNA damage e cell senescence [24].

ROS production of NHOSt cultured on HAPEI-PtR (3, 7 and 10 days), as well as on HAPEI-PtTT, (7 and 10 days) is significantly lower than on HA group ($p<0.05$), as shown in Figure 11. The culture with MG63 shows significantly lower values of ROS at 3 days for HAPEI-PtR and at 10 days for HAPEI-PtTT ($p<0.05$). The amount of ROMO1 producted by NHOst at 3 days on HAPEI-PtR and HAPEI-PtTT is higher than on HA ($p<0.05$). However, at 7 and 10 days the production in these same groups is significantly reduced when compared to HA ($p<0.05$) (Figure 11). The culture with MG63 shows very low production at 3 and 7 days in all groups. At 10 days there is a significant increase in HA group, whereas HAPEI-PtR and HAPEI-PtTT values remain low ($p<0.05$). Moreover, statistical analysis shows a correlation (Pearson test) between

ROS and ROMO1 production in both primary culture NHOst ($p<0.05$) and in MG63 cell lines ($p<0.005$).

4. Conclusions

In this work, Pt nanoparticles have been successfully supported on apatitic crystals. In particular, functionalization of hydroxyapatite nanocrystals with PEI has been shown to enhance PtNPs loading thanks to the polyelectrolyte interaction with the metallic ion, Pt(II). Chemical reduction results in the formation of nanometric PtNPs, whose dimensions on the apatitic supports significantly increase from ca. 1 nm to 20-30 nm after heat treatment. However, the good anti-oxidant properties of these composite materials are independent from metallic nanoparticles size, as shown by the similar values of H_2O_2 decomposing activity.

The cytoxicity of Pt(II) towards tumoral cells is maintained also when the metallic ion is supported on apatitic substrates. In fact, HAPEI-PtNR dramatically affects both SaOS2 and MG63 cell lines viability: the decrease is also due to membrane damage as stated by the high level of LDH release in medium at the end of experimental time.

The results of the investigation carried out on HAPEI-PtR and HAPEI-PtTT samples show that the proliferation and viability of primary osteoblasts is more sensible than those of an osteoblast cell line. However, both type of cells are well differentiated as demonstrated by significant stimulation of ALP activity (HAPEI-PtR and HAPEI-PtTT) and COL1a1 production (HAPEI-PtTT). Moreover, HAPEI-PtR as well as HAPEI-PtTT reduces the production of ROS and ROMO1, confirming the anti-oxidant action of these materials that contributes to counteract oxidative stress damage and cell senescence.

Acknowledgements

This work was supported by IRCCS Istituto Ortopedico Rizzoli (funds Ministero della Salute – Ricerca Corrente, and 5x1000/2017, code 730164) and the University of Bologna. The authors gratefully thank Dr. Francesca Bonvicini and Dr. Laura Sicuro for experimental support.

References

[1] S. Dasari, P.B. Tchounwou, Cisplatin in cancer therapy: molecular mechanisms of action, Eur. J. Pharmacol. 740 (2014) 364–378.

[2] W. Li, C. Liang, W. Zhou, J. Qiu, Z. Zhou, G. Sun, Q. Xin, Preparation and Characterization of multiwalled carbon nanotube-supported platinum for cathode catalysts of direct methanol fuel cells, J. Phys. Chem. B 107 (2003) 6292-6299.

[3] B.R. De Vasconcelos, L. Zhao, P. Sharrock, A. Nzihou, D.P. Minh, Catalytic transformation of carbon dioxide and methane into syngas over ruthenium and platinum supported hydroxyapatites, Appl. Surf. Sci. 390 (2016) 141–156.

[4] N. Takarroumt, M. Kacimi, F. Bozon-Verduraz, L.F. Liotta, M. Ziyad, Characterization and performance of the bifunctional platinum-loaded calcium-hydroxyapatite in the one-step synthesis of methyl isobutyl ketone, J. Mol. Catal. A: Chem. 377 (2013) 42– 50.

[5] M. Vukomanović, V. _Žunič, M. Otoničar, U. Repnik, B. Turk, S.D. Skapin, D. Suvorov, Hydroxyapatite/platinum bio-photocatalyst: a biomaterial approach to self-cleaning, J. Mater. Chem. 22 (2012) 10571-10580.

[6] M. Martins, C. Mourato, S. Sanches, J.P. Noronha, M.T. Barreto Crespo, I.A.C. Pereira, Biogenic platinum and palladium nanoparticles as new catalysts for the removal of pharmaceutical compounds, Water Res. 108 (2017) 160-168.

[7] S. Onizawa, K. Aoshiba, M. Kajita, Y. Miyamoto, A. Nagai, Platinum nanoparticle antioxidants inhibit pulmonary inflammation in mice exposed to cigarette smoke, Pulm. Pharmacol. Ther. 22 (2009) 340–349.

[8] H. Mohammadi, A. Abedi, A. Akbarzadeh, M.J. Mokhtari, H.E. Shahmabadi, M.R. Mehrabi, S. Javadian, M. Chiani, Evaluation of synthesized platinum nanoparticles on the MCF-7 and HepG-2 cancer cell lines, Int. Nano Lett. 3 (2013) 28 (5 pp.).

[9] W. Zheng, B. Jiang, Y. Hao, Y. Zhao, W. Zhang, X. Jiang, Screening reactive oxygen species scavenging properties of platinum nanoparticles on a microfluidic chip, Biofabrication 6 (2014), 045004 (11 pp.).

[10] M. Moglianetti, E.D. Luca, D. Pedone, R. Marotta, T. Catelani, B. Sartori, H. Amenitsch, S.F. Retta, P.P. Pompa, Platinum nanozymes recover cellular ROS homeostasis in an oxidative stress-mediated disease model, Nanoscale 8 (2016) 3739–3752.

[11] P. Puja, P. Kumar, A perspective on biogenic synthesis of platinum nanoparticles and their biomedical applications, Spectrochim. Acta Part A 211 (2019) 94–99.

[12] L. Zhang, L. Laug, W. Műnchgesang, E. Pippel, U. Gősele, M. Brandsch, M. Knez, Reducing Stress on Cells with Apoferritin-Encapsulated Platinum Nanoparticles, Nano Lett. 10 (2010) 219-223.

[13] H. Hosaka, R. Haruki, K. Yamada, C. Böttcher, T. Komatsu, Hemoglobin–Albumin Cluster Incorporating a Pt Nanoparticle: Artificial O_2 Carrier with Antioxidant Activities, PLoS ONE 9 (2014) e110541 (9 pp.).

[14] A Bigi, E Boanini, Calcium Phosphates as Delivery Systems for Bisphosphonates, J. Funct. Biomater. 9 (2018) 6 (18 pp.).

[15] D. Miao, A. Goldbach, H. Xu, Platinum/Apatite Water-Gas Shift Catalysts, ACS Catal. 6 (2016) 775−783.

[16] C. Chen, P. Kuo, Gold nanoparticles prepared using polyethylenimine adsorbed onto montmorillonite, J. Colloid Interf. Sci. 293 (2006) 101–107.

[17] X. Wang, Q. Liu, J. Liu, R. Chen, H. Zhang, R. Li, Z. Li, J. Wang, 3D self-assembly polyethyleneimine modified graphene oxide hydrogel for the extraction of uranium from aqueous solution, Appl. Surf. Sci. 426 (2017) 1063-1074.

[18] M. Thomas, Q. Ge, J.J. Lu, J. Chen, A.M. Klibanov, Cross-linked small polyethylenimines: while still nontoxic, deliver DNA efficiently to mammalian cells in vitro and in vivo, Pharm. Res. 22 (2005) 373–380.

[19] E. Boanini, P. Torricelli, F. Bonvicini, M.C. Cassani, M. Fini, G.A. Gentilomi, A. Bigi, A new multifunctionalized material against multi-drug resistant bacteria and abnormal osteoclast activity, Eur. J. Pharm. Biopharm. 127 (2018) 120–129.

[20] L. Forte, S. Sarda, P. Torricelli, C. Combes, F. Brouillet, O. Marsan, F. Salamanna, M. Fini, E. Boanini, A. Bigi, Multifunctionalization modulates hydroxyapatite surface interaction with bisphosphonate: antiosteoporotic and antioxidative stress materials, ACS Biomater. Sci. Eng. 57 (2019) 3429-3439.

[21] L. Forte, S. Sarda, C. Combes, F. Brouillet, M. Gazzano, O. Marsan, E. Boanini, A. Bigi, Hydroxyapatite Functionalization to Trigger Adsorption and Release of Risedronate, Colloids Surf. B 160 (2017) 493−499.

[22] B.L. Rivas, S.A. Pooley, E.D. Pereira, R. Cid, M. Luna, M.A. Jara, K.E. Geckeler,Water-soluble amine and imine polymers with the ability to bind metal ions in conjunction with membrane filtration, J. Appl. Polym. Sci. 96 (2005) 222-231.

[23] P.D. Ray, B.W. Huang, Y. Tsuji,Reactive oxygen species (ROS) homeostasis and redox regulation in cellular signaling, Cell Signal. 24 (2012) 981–990.

[24] G.Y. Lee, D.G. You, H.R. Lee, S.W. Hwang, C.J. Lee, Y.D. Yoo, Romo1 is a mitochondrial nonselective cation channel with viroporin-like characteristics, J. Cell Biol. 217 (2018) 2059–2071.

Captions to the figures

Figure 1. Comparison of HA and HAPEI samples: (a) X-ray diffraction patterns; (b) TGA weight loss curves (solid lines) and related first derivatives (dashed lines).

Figure 2. Scheme of the synthetic pathways: the loading of Pt(II) ions can give rise to the formation of supported PtNPs, both on HA or HAPEI crystals as supports, but in different amounts. The dimensions of PtNPs increase after thermal treatment (PtTT).

Figure 3. TEM images of Pt nanoparticles supported on HA or HAPEI (HA-PtR and HAPEI-PtR) and of Pt nanoparticles supported on HAPEI after heat treatment at 700 °C (HAPEI-PtTT); scale bars = 100 nm.

Figure 4. X-ray diffraction patterns of HA and HAPEI crystals loaded with Pt(II) (HA-PtNR and HAPEI-PtNR), and with Pt nanoparticles before (HA-PtR and HAPEI-PtR) and after heat treatment (HA-PtTT and HAPEI-PtTT). Platinum peaks are indicated with *.

Figure 5. Activities of HAPEI, HAPEI-PtR and HAPEI-PtTT for the H2O2 decomposition at 37 °C and pH 7.4.

Figure 6. SaOS2 and MG63 viability (c-d) and LDH (e-f) after 48 hours of incubation with HAPEI-PtNR, reference HA and CTR (cells only). Results of Alamar blue dye are reported as relative fluorescence units (RFU). Values of LDH are normalized to viability (LDH/Alamar). Statistical analysis to detect differences among groups is reported in the figure (*p<0.05,**p<0.005,***p<0.0005): *HA vs CTR-; ***,** HAPEI-PtNR vs HA, CTR-).

Figure 7. Live/Dead® assay. Significant images of MG63 (a) and of SaOS2 (b) grown in direct contact on HA and on HAPEI-PtNR. Living cells are green, dead cells are red (magnification 4x).

Figure 8. NHOst and MG63 viability after 3, 7and 10 days of culture on HAPEI-PtR, HAPEI-PtTT and HA as reference. Results of Alamar blue dye are reported as relative

fluorescence units (RFU). Statistical analysis is reported in the figure (*p<0.05, **p<0.005).
NHOst 3, 7, and 10 days: **HAPEI-PtR vs HA, HAPEI-PtTT;
MG63 10 days: *HAPEI-PtTT vs HA.

Figure 9. Live/Dead® assay. Significant images of NHOst and MG63 grown in direct contact of HA, HAPEI-PtR and HAPEI-PtTT (magnification 20x). The green living cells regularly colonized sample surface and their density correlate with viability data (figure 7).

Figure 10. Evaluation of cell activity and differentiation (ALP, ng/ml; COL1a1, pg/ml) measured in supernatant of NHOst and MG63 osteoblasts grown on biomaterials after 3, 7 and 10 days of culture. The statistical analysis, performed to detect significant differences between groups (* p<0.05), is reported in the figure.
NHOst ALP 3 days: *HA vs HAPEI-PtR, HAPEI-PtTT; * HAPEI-PtTT vs HAPEI-PtR; 7 days: *HA vs HAPEI-PtR, HAPEI-PtTT;
MG63 ALP 3, 10 days: *HA vs HAPEI-PtR, HAPEI-PtTT; 7 days: * HAPEI-PtR vs HA, HAPEI-PtTT;
NHOst COL1a1 3 days: *HA vs HAPEI-PtR, HAPEI-PtTT; 7 days: * HAPEI-PtR vs HA, HAPEI-PtTT; 10 days: * HAPEI-PtR vs HA, HAPEI-PtTT; * HAPEI-PtTT vs HA;
MG63 COL1a1 3, 7 and 10 days: * HAPEI-PtTT vs HA, HAPEI-PtR.

Figure 11. Evaluation of ROS (IU/ml) and ROMO1 (pg/ml) as cell response to stress oxidative measured in supernatant of NHOst and MG63 osteoblasts grown on biomaterials after 3, 7 and 10 days of culture. The statistical analysis, performed to detect significant differences between groups (* p<0.05), is reported in the figure.
NHOst ROS 3 days: * HAPEI-PtR vs HA, HAPEI-PtTT; 7 days: *HA vs HAPEI-PtR, HAPEI-PtTT; 10 days: *HA vs HAPEI-PtR, HAPEI-PtTT;
MG63 ROS 3 days: *HAPEI-PtR vs HA, HAPEI-PtTT; 10 days: HAPEI-PtTT vs HA, HAPEI-PtR;
NHOst ROMO1 3 days: *HA vs HAPEI-PtR, HAPEI-PtTT; 7 days: * HAPEI-PtTT vs HA; 10 days: *HA vs HAPEI-PtR, HAPEI-PtTT;
MG63 ROMO1: 10 days: *HA vs HAPEI-PtR, HAPEI-PtTT

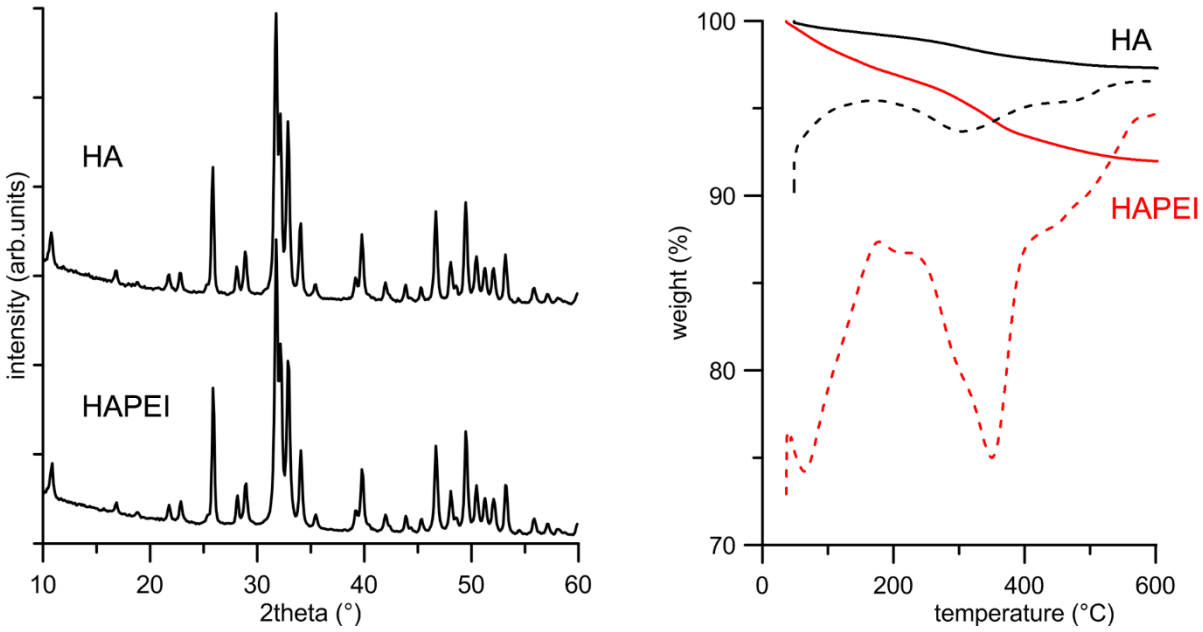

Figure 1

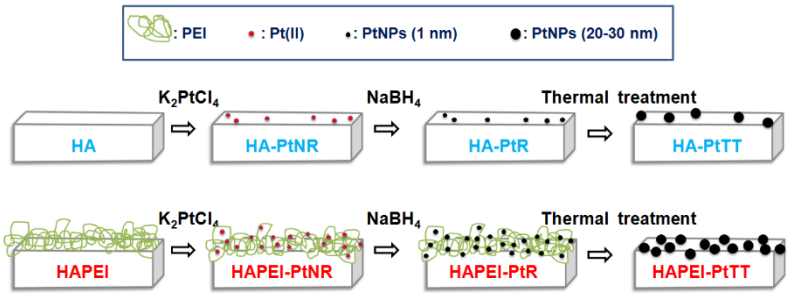

Figure 2

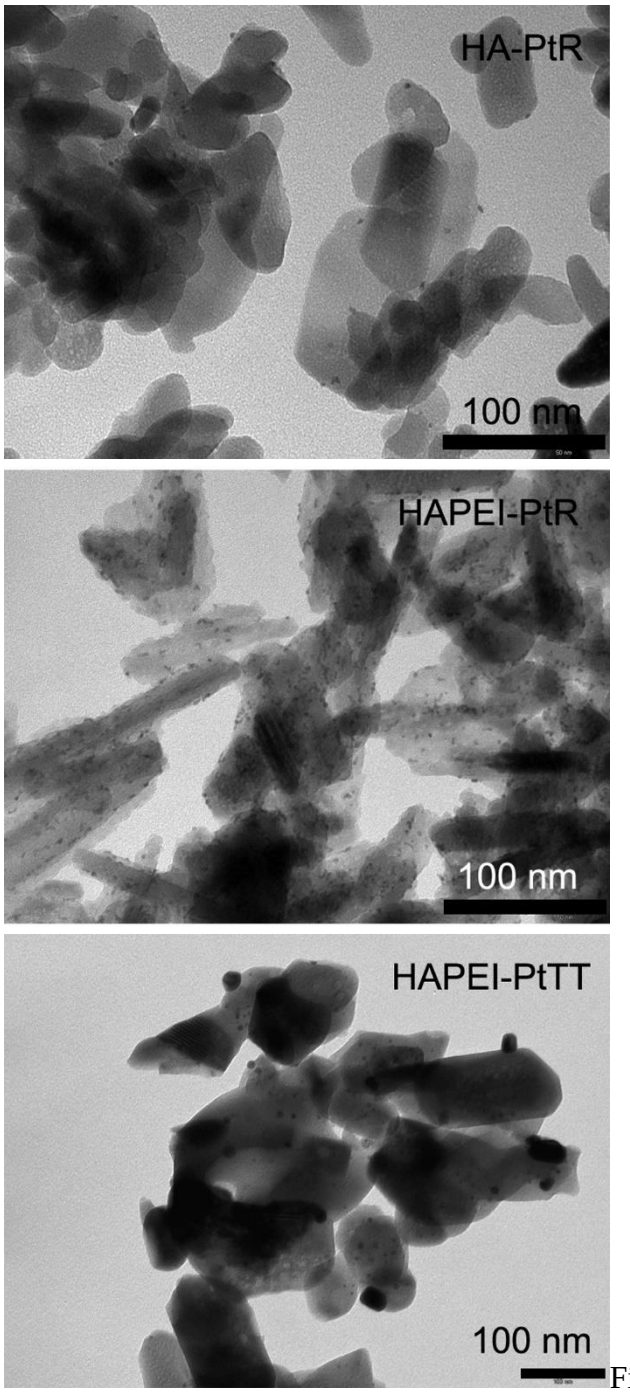

Figure 3

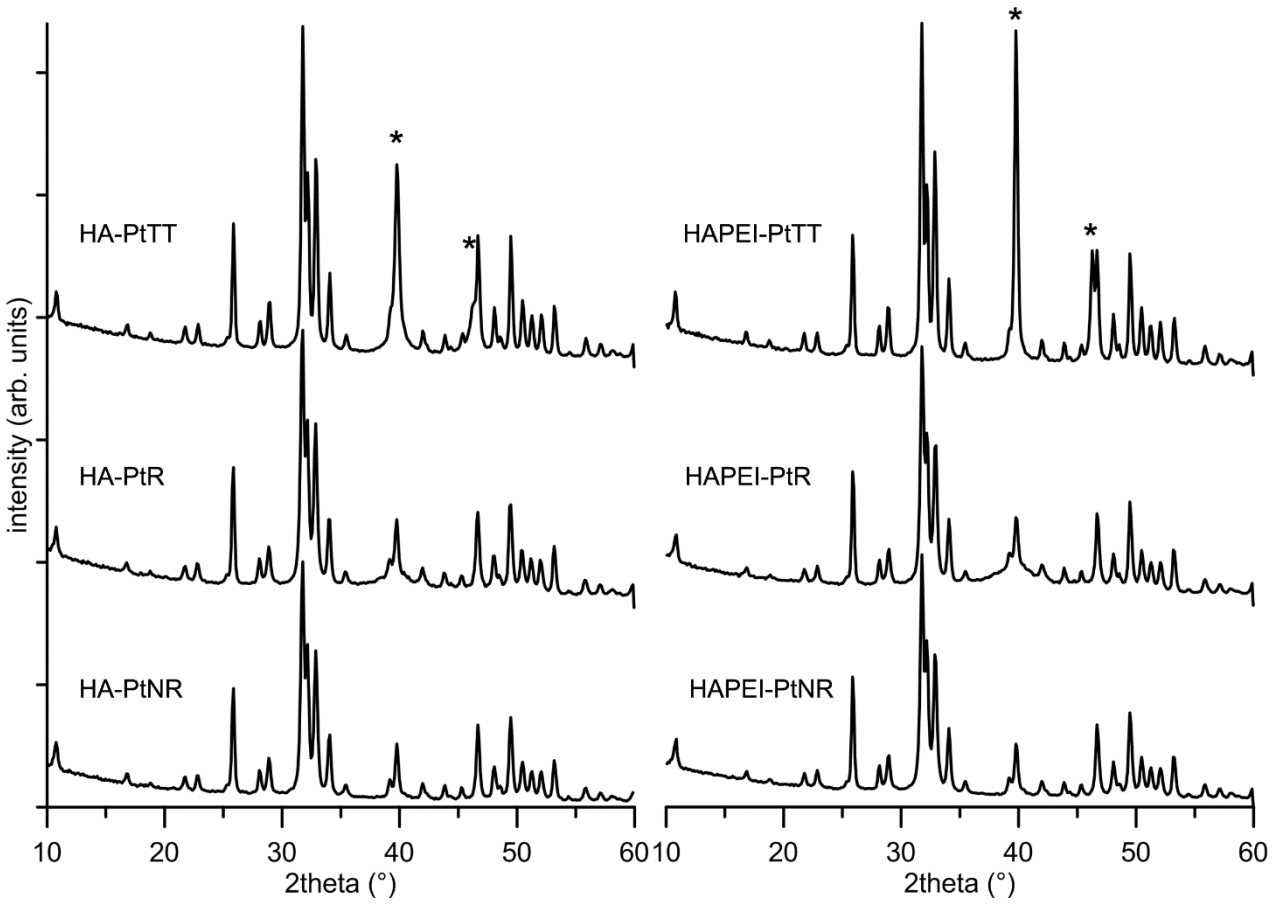

Figure 4

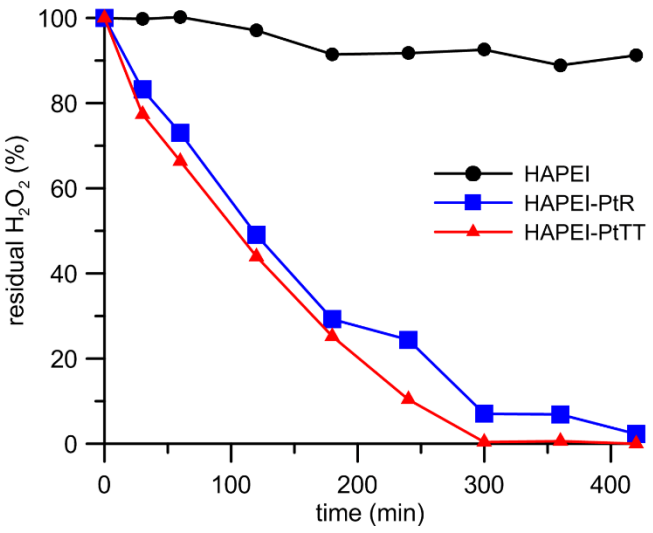

Figure 5

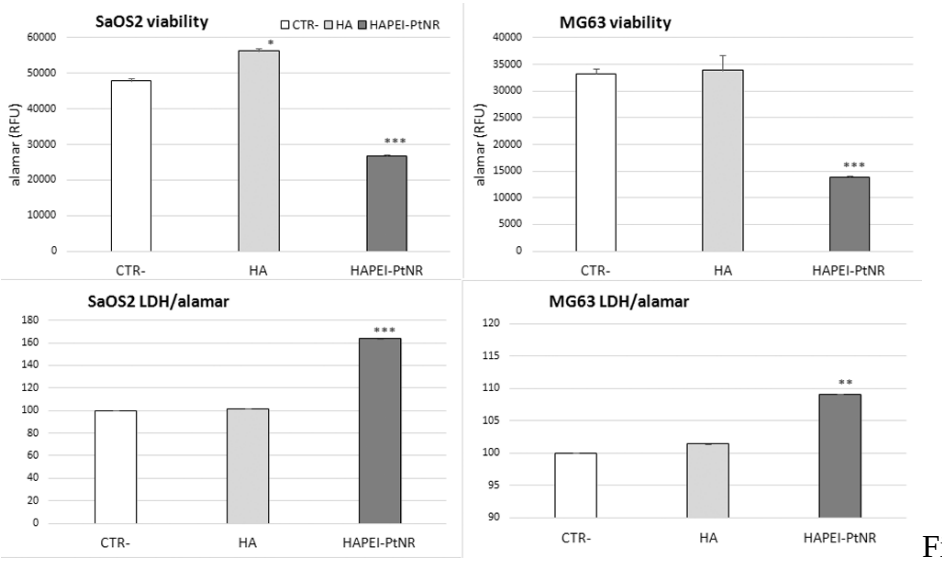

Figure 6

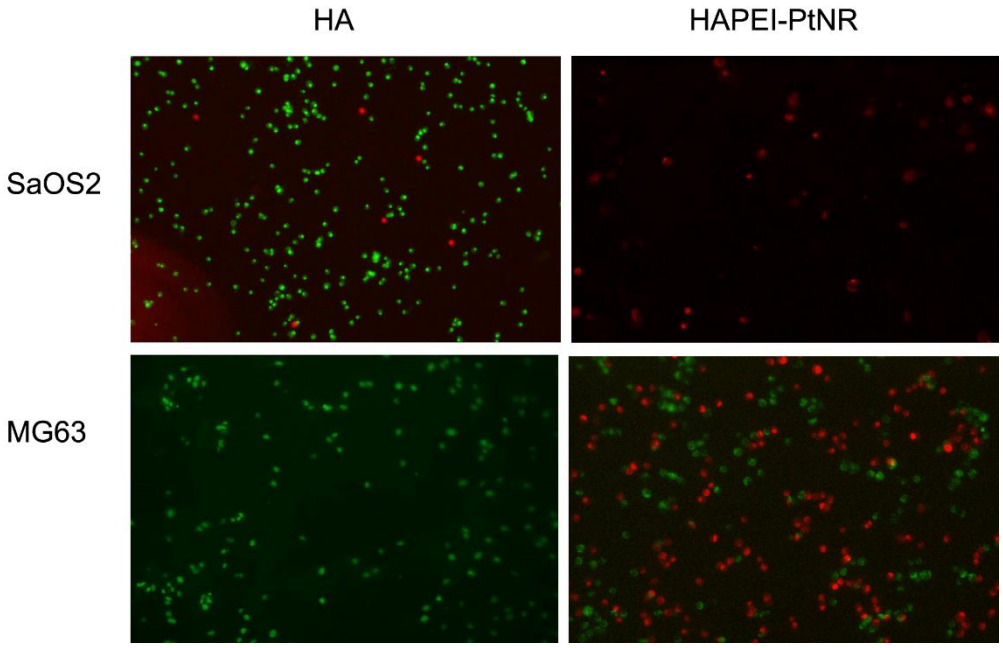

Figure 7

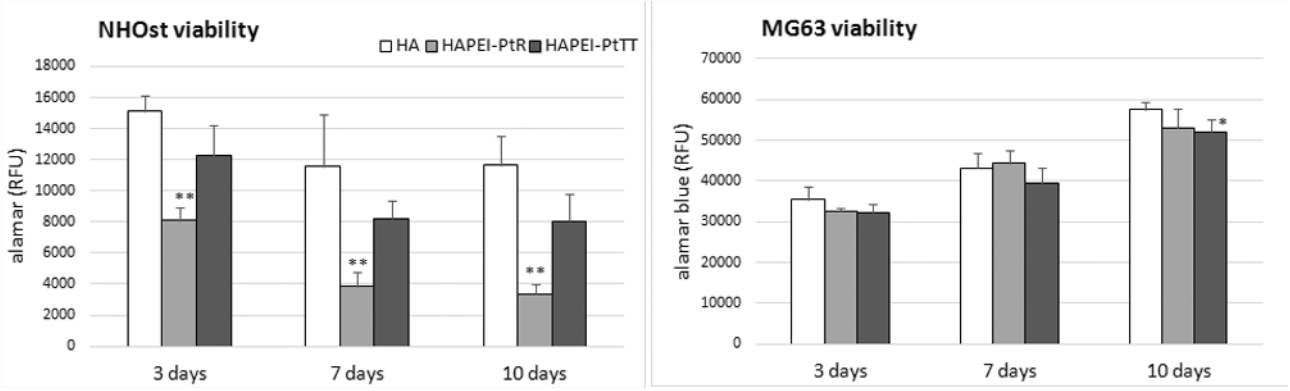

Figure 8

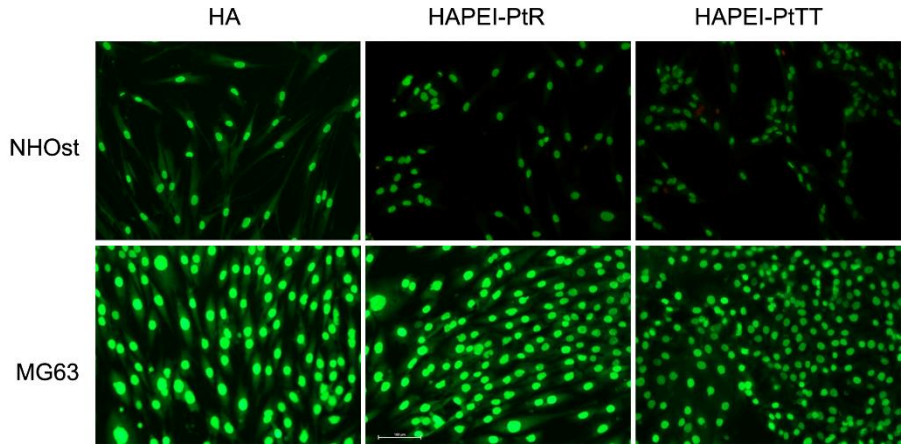

Figure 9

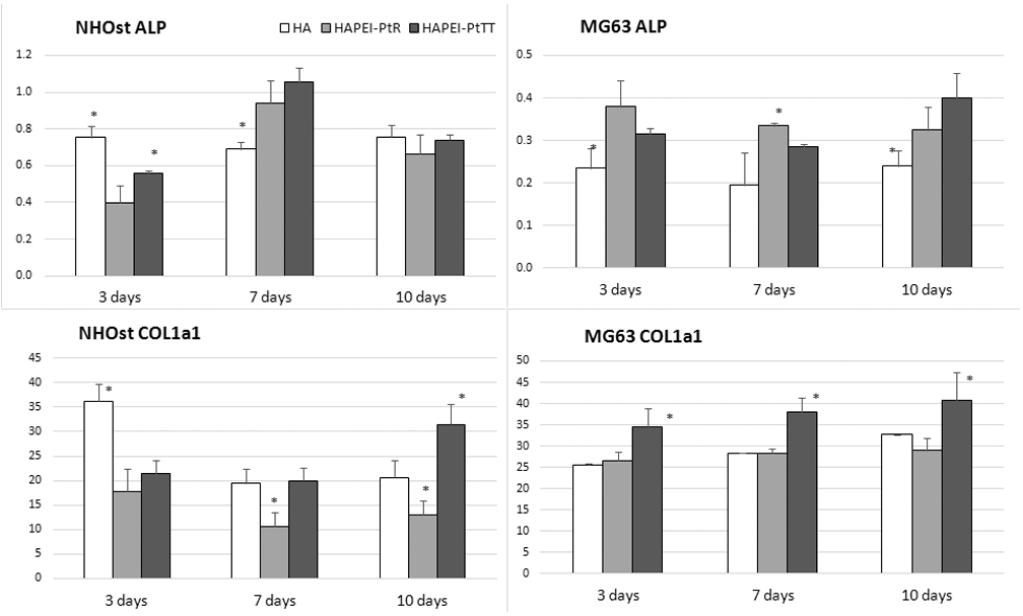

Figure 10

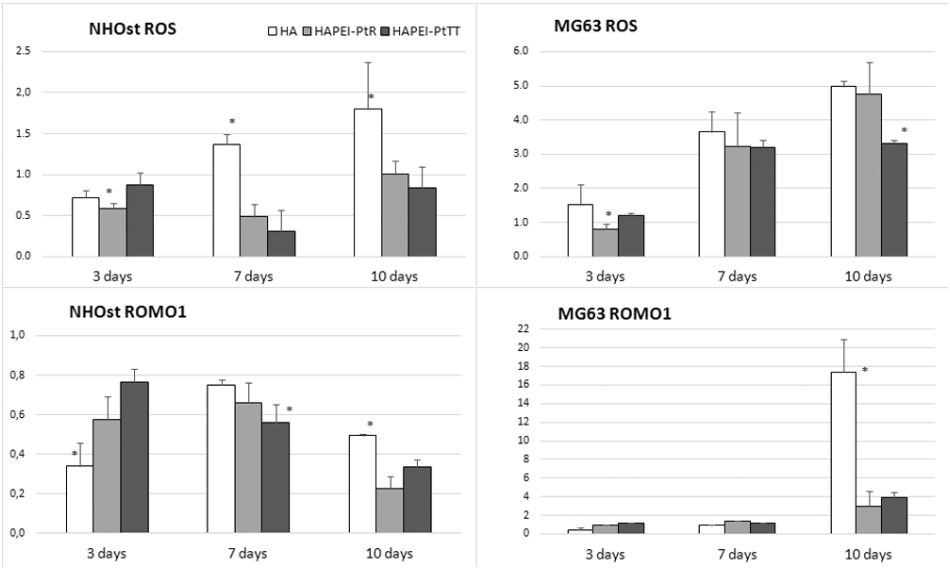

Figure 11